Emergent Structures in an Active Polar Fluid: Dynamics of Shape, Scattering, and Merger

Kabir Husain and Madan Rao*
Simons Centre for the Study of Living Machines, National Centre for Biological Sciences (TIFR), Bellary Road, Bangalore 560 065, India
(Received 30 April 2016; published 17 February 2017)

Spatially localized defect structures emerge spontaneously in a hydrodynamic description of an active polar fluid comprising polar "actin" filaments and "myosin" motor proteins that (un)bind to filaments and exert active contractile stresses. These emergent defect structures are characterized by distinct textures and can be either static or mobile—we derive effective equations of motion for these "extended particles" and analyze their shape, kinetics, interactions, and scattering. Depending on the impact parameter and propulsion speed, these active defects undergo elastic scattering or merger. Our results are relevant for the dynamics of actomyosin-dense structures at the cell cortex, reconstituted actomyosin complexes, and 2D active colloidal gels.

DOI: 10.1103/PhysRevLett.118.078104

The dynamical interplay between topological defects, elasticity, and flow has been a recurrent theme in the physics of condensed media [1]. This has been of recent interest in the context of active systems, in which activity drives the formation and dynamics of collective or emergent structures [2]: be it the rotation of spiral defects in polar gels [3,4], the translation, ordering, and complex flows of $+1/2$ disclinations in active nematics composed of filament-motor complexes [5–13] or the spontaneous formation of interacting mobile aggregates of active colloidal particles [14–18]. These structures are often particlelike, with a well-defined position and orientation, and it is desirable to cast their dynamics solely in terms of their own coordinates and form factor.

In this Letter we analyze the emergent dynamics of polar filaments ("actin") actively driven by motor proteins ("myosin") that undergo turnover, i.e., binding or unbinding (with an estimated time scale of ~6 s *in vivo* [19]) [20–23]. Recent studies on actomyosin-dependent molecular clustering at the cell surface and in *in vitro* reconstitutions of a thin actomyosin layer on a supported membrane, provide our primary motivation [20,24–26]. Our main results are the following: (i) A variety of spatially compact structures, such as mobile virtual defects, rotating spiral defects, or stationary asters, emerge spontaneously from an interplay between elastic, dissipative, and active stresses. (ii) Activity drives defect motion and shape deformation, with isolated virtual defects moving as extended particles, dressed by a cloud of myosin density. (iii) These extended particles interact via the accompanying myosin cloud, and exhibit both *phoresis* and *taxis*. (iv) We study the dynamics, elastic scattering, and (inelastic) merger of a pair of mobile defects as a function of impact parameter and self-propulsion velocity, by casting the effective dynamics in terms of defect coordinates and shape factor. We note that all the emergent characteristics of the extended particle—its integrity, dynamics, and their mutual interactions, are consequences of the dressed myosin cloud.

Our results are obtained by solving hydrodynamic equations for a thin film of active fluid comprising actin filaments, described by a concentration c and orientation $\mathbf{n}$, and filament-bound myosin motors, with concentration ρ, which dissipate momentum via frictional damping at the cell substrate. As found from systematic coarse grainings [21], the active contributions to the dynamics of c and $\mathbf{n}$ come about only in the presence of bound myosin—the Supplemental Material [27] contains a phenomenological derivation of the following simplified hydrodynamic equations, based on symmetry and conservation laws [4,30],

$$\frac{\partial c}{\partial t} = -\vec{\nabla}\cdot(-D_a\vec{\nabla}c + v_0 c\mathbf{n} - Wc\vec{\nabla}\rho), \tag{1}$$

$$\frac{\partial \rho}{\partial t} = -\vec{\nabla}\cdot(-D_m\vec{\nabla}\rho + v_0\rho\mathbf{n}) + k_b\frac{c}{c+c_h} - k_u\rho \tag{2}$$

$$\frac{\partial \mathbf{n}}{\partial t} + \lambda(\rho)(\mathbf{n}\cdot\vec{\nabla})\mathbf{n} = K\nabla^2\mathbf{n} - \zeta_0\vec{\nabla}c + \zeta\vec{\nabla}\rho + [\alpha(c) - \beta(c)n^2]\mathbf{n}, \tag{3}$$

where we have taken the active stress $\boldsymbol{\sigma}^{\mathrm{act}} = -W(c)\rho$ ($W < 0$, for contractility), and we work in the one-constant approximation [31]. We take $\alpha(c) = \nu(c/c_* - 1)$ and $\beta(c) = \nu(1 + c/c_*)$, which ensures that $|\mathbf{n}|^2 \to 1$, when $c \gg c_*$ [32]. In Eq. (3), $\zeta_0 > 0$ ensures positive filament compressibility, while $\zeta > 0$ describes the preferential alignment of the filament orientation to gradients of myosin density [23], here a consequence of the active stress. These equations generalize earlier models of acto-myosin [20–23,32], which had been proposed on the strength of both symmetry arguments and coarse grainings, by explicitly treating both the polar filaments and the myosin motors as dynamical variables. We note a resemblence to recently

proposed models of chemoactive colloids [33], which suggests that our results may be of wider applicability.

We begin by studying the linear instability of the homogeneous, orientationally isotropic phase when $c_0 < c_*$, under the perturbations, $c(\mathbf{r},t) = c_0 + \delta c(\mathbf{r},t)$, $\rho(\mathbf{r},t) = \rho_0 + \delta\rho(\mathbf{r},t)$ and $\mathbf{n}(\mathbf{r},t) = \delta\mathbf{n}(\mathbf{r},t)$, where $\rho_0 = (c_0/c_0 + c_h)k_b/k_u$. We find two potential instability mechanisms. (i) The binding of myosin and the contractile advection of filaments ($\propto Wc\vec{\nabla}\rho$) induces an density clumping instability when $k_b|W| \gtrsim D_a k_u$, with a band of unstable wave vectors between $k = 0$ and $k = \sqrt{|W|k_b c_0 - D_a k_u}/D_a$. Filament orientation remains disordered ($\langle\mathbf{n}\rangle = 0$). (ii) Myosin-induced torques ($\propto \zeta\vec{\nabla}\rho$) and advection ($\propto v_0 c\mathbf{n}$) drives a splay deformation ($|\vec{\nabla}\cdot\mathbf{n}| > 0$) and density clumping when $D_a|\alpha(c_0)| \lesssim v_0\zeta\rho_0$, with a band of unstable wave vectors between $k = 0$ and $k = \sqrt{[D_a k_u \alpha(c_0) + c_0 k_b v_0 \zeta]/[D_a K k_u]}$. In both cases the instability towards clumping is non-oscillatory [27].

To see the fine structure of the emergent compact configurations, we need to go beyond the linear regime. We numerically integrate Eqs. (1)–(3) on a square grid with periodic boundary conditions using an explicit forward-time-central-space (FTCS) scheme and appropriate initial conditions [27]. Starting from a homogeneous, isotropic phase, we observe that the system quickly settles down into an evolving population of spatially compact actin-myosin clusters (Supplemental Material, movies 1, 2 [27]). To explore the typology of compact structures formed, we choose initial conditions that produce a single defect and build a phase diagram in K and ζ.

Figure 1(a) shows the single-defect phase diagram together with the compact density profiles and orientational textures that we obtain. All structures consist of a compact accumulation of actin filaments dressed by a wider myosin cloud [Fig. 1(b)]. At low K they are radially symmetric with zero net polarity ($\langle c\mathbf{n}\rangle = 0$) and, hence, static. The texture is set by the control parameter ζ/ζ_0. When ζ/ζ_0 is small (large) the term $\zeta_0\vec{\nabla}c$ ($\zeta\vec{\nabla}\rho$) dominates to form an out(in)-pointing aster. As we show in the Supplemental Material [27], integrating out the myosin density when it is "fast," in the limit of large ζ/ζ_0, results in effective equations for the active filament identical to those analyzed in [20,34], with a "negative compressibility" in the $\mathbf{n}$ equation [32,34].

At an intermediate value of ζ/ζ_0, $\zeta_0\vec{\nabla}c$ dominates at the core of the domain and $\zeta\vec{\nabla}\rho$ dominates at the boundary, forming a spiral aster texture, which rotates with an angular velocity $\omega(r) \propto v_0 n_\theta(r)$ [3,4].

When K is large the defect core moves abruptly from within to outside the compact domain, giving rise to an apparent or virtual defect [35–37]. Depending on the relative strength of $\zeta\vec{\nabla}\rho$ and $\zeta_0\vec{\nabla}c$, the virtual defect is either a virtual out-pointing aster ($\langle c\vec{\nabla}\cdot\mathbf{n}\rangle > 0$) or a virtual aster ($\langle c\vec{\nabla}\cdot\mathbf{n}\rangle < 0$).

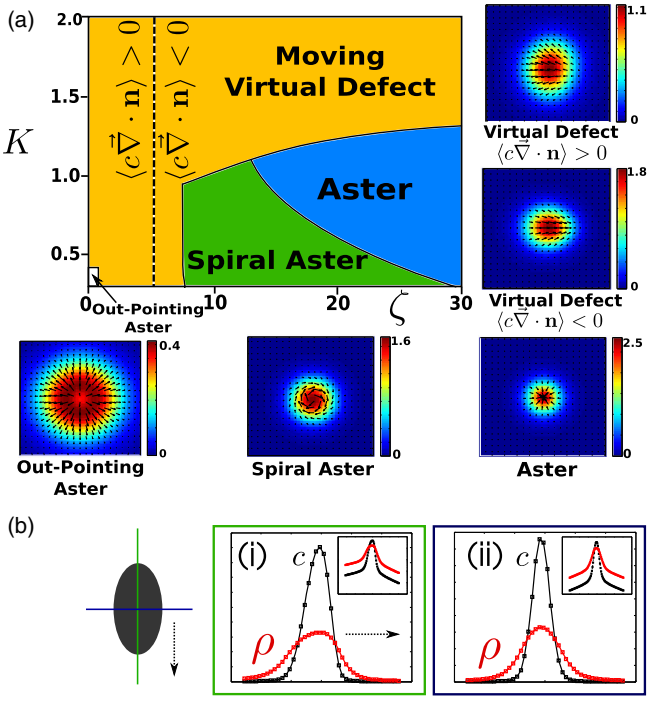

FIG. 1. (a) Typology of spatially compact single-defect structures in the K—ζ plane for a fixed concentration of filaments c_0, together with snapshots of the textures formed by the filament orientation $\mathbf{n}$—the heat map represents c and the arrows represent $c\mathbf{n}$. All snapshots are equally sized. (b) Myosin (red) and actin (black) concentration profiles within a moving virtual aster, along directions (i) longitudinal and (ii) transverse to the direction of motion (dashed arrow). Insets: semilog scale.

These textures can be qualitatively understood as arising from a competition between the first three terms on the right-hand side of Eq. (3). We further note that the dynamics of $\mathbf{n}$ (when $\lambda = 0$) can be obtained as $\partial_t\mathbf{n} = -\delta\mathcal{L}/\delta\mathbf{n}$, where the Lyapunov function $\mathcal{L} = \int d^2x\,[K(\partial_i n_j)(\partial_i n_j) + (\zeta\rho - \zeta_0 c)\vec{\nabla}\cdot\mathbf{n}]$. The quantity $\zeta\rho - \zeta_0 c$ thus promotes a spontaneous splay [37,38], with a negative (positive) divergence when $\zeta\rho - \zeta_0 c > 0$ (< 0). The Lyapunov function $\mathcal{L}$ is analogous to the free energy of textured Langmuir domains [35,37], indicating that the transition between aster and virtual defect is first order, as a function of the control parameter $R_a(\zeta\rho_0 - \zeta_0 c_0)/K$ [35], where R_a is the radius of the filament domain.

The profile of filament and myosin densities is set by the interplay between the binding and advective nonlinearities and it is difficult to obtain an exact expression. However, we may exploit the compactness of the filament domain to analyse the decay of the dressed cloud of myosin. Compactness implies that $c(\mathbf{r})$, $|\mathbf{n}| \approx 0$ for $r > R_a$ (where R_a is naturally interpreted as the radius of the filament domain). The outer solution (i.e., for $r > R_a$) for ρ at steady state satisfies $D_m\nabla^2\rho = k_u\rho$. The radially symmetric solution is found to be,

$$\rho(r) = A_1 K_0(r/r_0), \tag{4}$$

where $K_\nu(r)$ is the modified Bessel function of the second kind and $r_0 = \sqrt{D_m/k_u}$. The constant A_1 may be determined by matching the inner solution ($r < R_a$, where $|\mathbf{n}|$, $c \geq 0$) with the outer solution.

The sudden appearance of a net polarity ($|\langle c\mathbf{n}\rangle| > 0$) manifests as a shape distortion away from circularity and a center-of-mass motion driven by the advective current, $\propto c\mathbf{n}$, which we analyze to lowest order in deformation. We transform to a comoving frame with velocity $\mathbf{v_c}$ and solve for the lowest order axisymmetric steady-state solution, i.e., of the form $\rho_0(r) + \rho_1(r)\cos\theta$, where $\theta = 0$ is the direction of motion. When deviations from circularity are small ($\rho_1 \ll \rho_0$), ρ_0 is given by Eq. (4) and,

$$\rho_1(r) = A_2 K_1\left(\frac{r}{r_0}\right) - \frac{v_c}{\sqrt{D_m k_u}} A_1 r K_0\left(\frac{r}{r_0}\right), \qquad (5)$$

where A_2 may once again be obtained from matching the inner and outer solutions at $r = R_a$.

From our numerical analysis, we find that an isolated moving virtual defect with its myosin cloud maintains its shape and texture over time. The density and orientation fields then obey a traveling front form $c = c[\mathbf{r} - \mathbf{R}(t)]$, $\mathbf{n} = \mathbf{n}[\mathbf{r} - \mathbf{R}(t)]$, $\rho = \rho[\mathbf{r} - \mathbf{R}(t)]$. We may thus describe the motion of a single virtual defect, isolated from others, solely in terms of its center-of-mass coordinate $\mathbf{R}(t) \equiv c_t^{-1}\int_\Omega d^2r\,\mathbf{r}c$ and net polarity $\mathbf{p}(t) \equiv c_t^{-1}\int_\Omega d^2r\,\mathbf{n}c$, where $c_t = \int_\Omega d^2r\,c$ and Ω is the compact support of the defect,

$$\dot{\mathbf{R}}(t) = \frac{1}{c_t}\int d^2r\,\mathbf{J_f} \approx \frac{v_0}{c_t}\int d^2r\,c\mathbf{n} = v_c\hat{\mathbf{p}}(t),$$
$$\dot{\mathbf{p}}(t) = \frac{1}{c_t}\int d^2r\,c\underbrace{\left(\frac{\mathbf{J_f}}{c}\cdot\vec{\nabla} + \frac{\partial}{\partial t}\right)}_{\text{convective derivative}}\mathbf{n} = 0, \qquad (6)$$

where the overdot is a time derivative. Above, we have made use of the fact that filament diffusion $D_a\vec{\nabla}c$ and the $Wc\vec{\nabla}\rho$ term are responsible for maintaining the size of the moving domain, and, hence, they balance to 0 everywhere. This leaves only the advective contribution ($\propto v_0 c\mathbf{n}$) in the first equation.

The speed of the domain, $v_c = v_0|\mathbf{n}^c|$, may be approximately calculated from an ansatz [shown in Fig. S3(b) in Ref. [27]] and is found to increase from $\sim 0.85 v_0$ to v_0 as the apparent defect core moves further from the center of the domain. This is consistent with the numerics [27], though we note that the asymmetric profile of the filament and myosin fields will also contribute to the speed of the domain.

We next investigate the interaction between these "particles." When the filament cores of two domains are well-separated, $|\mathbf{n}| \approx 0$ in the region between them and elastic interactions may be neglected. Their interaction is instead mediated by the associated myosin clouds—stationary defects do not interact unless they are close enough to allow for a finite overlap between their myosin clouds, with a interaction length scale $r_0 = \sqrt{D_m/k_u}$—this interaction leads to their merger (Supplemental Material, movie 1 [27]). On the other hand, moving virtual defects may initially be well separated and then approach each other (Supplemental Material, movie 2 [27]). We derive interactions between virtual defects by decomposing the microscopic fields into their contributions from the each domain ($c = \sum c_i$, etc.), valid when the domains are well separated ($|\mathbf{R_i} - \mathbf{R_j}| > R_a$), and define the center of mass and polarity of the each cluster ($\mathbf{R}_i$ and $\mathbf{p}_i$) as before:

$$\dot{\mathbf{R}}_i(t) = v_c\mathbf{p}_i(t) - \sum_{j\neq i}\frac{W}{c_t^{(i)}}\int d^2r\,c_i(\mathbf{r})\vec{\nabla}\rho_j(\mathbf{r} - \mathbf{R}_j),$$
$$\dot{\mathbf{p}}_i(t) = \sum_{j\neq i}\frac{\zeta}{c_t^{(i)}}\int d^2r\,c_i(\mathbf{r})\vec{\nabla}\rho_j(\mathbf{r} - \mathbf{R}_j). \qquad (7)$$

The second equation must be augmented with the constraint that the magnitude of each $\mathbf{p}_i$ is constant.

We develop the integral appearing in both equations into a multipole expansion, valid when the length scale over which the myosin cloud varies, r_0, is larger than the characteristic size of the virtual defect. Expanding $\rho_j(\mathbf{r} - \mathbf{R}_j)$ around $\mathbf{r} = \mathbf{R}_i$ we find

$$\int d^2r\,c_i(\mathbf{r})\,\vec{\nabla}\rho_j(\mathbf{r} - \mathbf{R}_j)$$
$$= M^{(0)}\vec{\nabla}\rho_j(\mathbf{R}_{ij}) + (\mathbf{M}^{(2)}(\mathbf{R}_i):\vec{\nabla}\,\vec{\nabla})\vec{\nabla}\rho_j(\mathbf{R}_{ij}) + \cdots, \quad (8)$$

where the multipole moments are $M^{(0)} = \int d^2r\,c_i(\mathbf{r})$ and $M^{(2)}_{\alpha\beta}(\mathbf{r}') = \frac{1}{2}\int d^2r(r_\alpha - r'_\alpha)(r_\beta - r'_\beta)\,c(\mathbf{r})$. Expanding the myosin field into axisymmetric circular harmonics $\rho(\mathbf{R}) = \rho^{(0)}(R) + \rho^{(1)}(R)(\mathbf{p}\cdot\mathbf{R}/R) + \cdots$ and using the forms given in Eqs. (4), (5), we may close the effective equations of motion for a population of interacting virtual defects. Retaining for simplicity only the radially symmetric term in ρ [i.e., Eq. (4) and the monopole term in Eq. (8)], and using the shorthand $\mathbf{R}_{ij} = \mathbf{R}_i - \mathbf{R}_j$:

$$\dot{\mathbf{R}}_i(t) = v_c\mathbf{p}_i(t) - \sum_{j\neq i}\frac{WA_1}{r_0}\mathrm{K}_1\left(\frac{|\mathbf{R}_{ij}|}{r_0}\right)\hat{\mathbf{R}}_{ji},$$
$$\dot{\mathbf{p}}_i(t) = \sum_{j\neq i}\frac{\zeta A_1}{r_0}\mathrm{K}_1\left(\frac{|\mathbf{R}_{ij}|}{r_0}\right)\hat{\mathbf{R}}_{ji}\cdot(\mathbb{1} - \mathbf{p}_i\mathbf{p}_i). \qquad (9)$$

Note that, as each ρ_j decays away from R_j, the signs of W and ζ give rise to an attractive "force" (*phoresis*) and an attractive "torque" (*taxis*), respectively, between virtual defects [39,40]. We note that while only a virtual defect may exhibit taxis (which requires a nonzero $\mathbf{p}$) the imposition of a gradient of myosin motors may elicit the phoresis of an otherwise static aster (Supplemental Material, movie 7 [27]).

We now turn to the consequences of Eqs. (7) and (8) on the "scattering" of virtual defects. First, we investigate this in the geometry depicted in Fig. 2(b) by numerically integrating

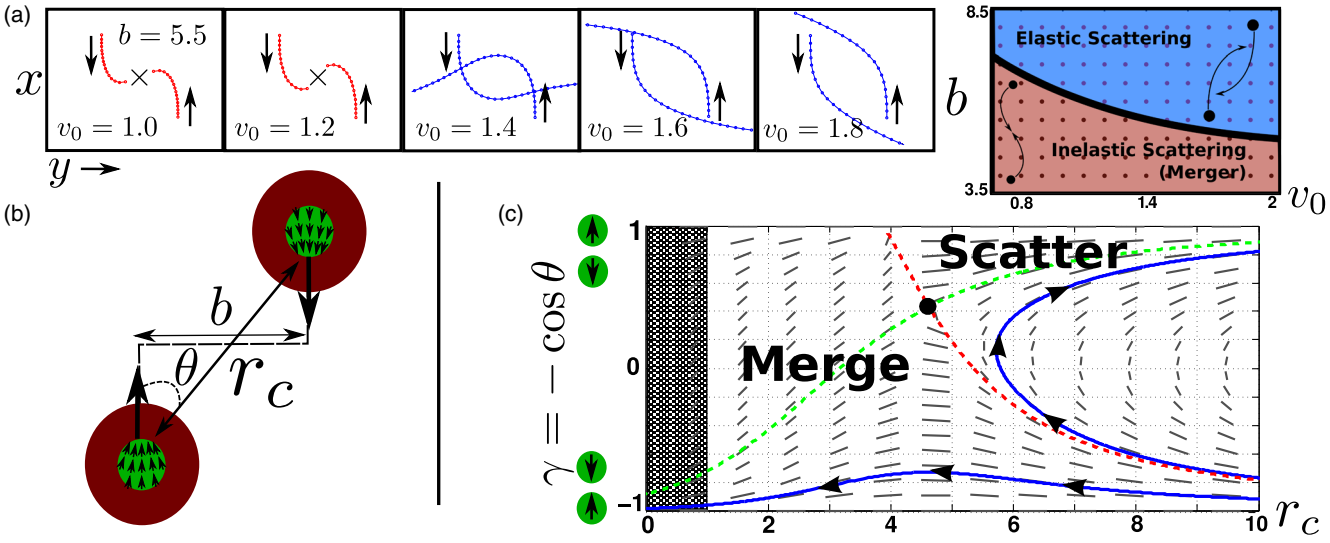

FIG. 2. (a) Left: several representative trajectories from the numerics with varying v_0 and fixed $b = 5.5$ (merger is depicted by the ×). Right: The outcome as a function of impact parameter b and self-advection v_0. (b) Left: The scattering geometry (green: c, arrows: $\mathbf{n}$, red: ρ). (c) The phase portrait of the scattering dynamical system, Eqs. (10), generated using the software PPLANE [41]. The black dot is the saddle point whose unstable separatrix (red dashed line) separates the merge region from the scattering region. Plotted in green is the stable separatrix. In blue are two example trajectories. The shaded region is the distance at which the merger will occur.

the full equations of motion, Eqs. (1)–(3). Figure 2(a) shows that for large impact parameter b or for large self-propulsion speed $\propto v_0$ the two clusters "elastically scatter" off each other and escape to the far field (Supplemental Material, movie 3 [27]), whereas for low b or low v_0 they merge (Supplemental Material, movie 4 [27]). Interestingly, as seen in the trajectories shown in Fig. 2(a), the deflection angle of scattering decreases with v_0 even for a fixed b. This is reminiscent of the scattering of inertial particles, even though the extended particles here are formed by constituents undergoing overdamped dynamics.

The symmetry of the scattering geometry of Fig. 2(b) can be exploited to develop an analytic representation of the scattering process. We define the distance of one virtual defect from the other, $r_c = |\mathbf{R}_{21}|$, and the radial projection of the polarity vector, $\gamma = \mathbf{R}_{12} \cdot \mathbf{p}_1 / r_c$.

$$\dot{r}_c = 2v_c\gamma + 2\bar{W}\mathrm{K}_1\left(\frac{r_c}{r_0}\right),$$
$$\dot{\gamma} = (1-\gamma^2)\left[2\frac{v_c}{r_c} - \bar{\zeta}\mathrm{K}_1\left(\frac{r_c}{r_0}\right)\right], \qquad (10)$$

where $\bar{W} = WA_1/r_0$ and $\bar{\zeta} = \zeta A_1/r_0$.

A representative phase portrait of this dynamical system is depicted in Fig. 2(c). It can be shown that Eqs. (10) admit a single saddle node [42], which is always between $0 < \gamma \leq 1$. Thus, in the physically relevant region of the phase plane $-1 < \gamma < 1$, the unstable separatrix of this saddle node acts as a phase boundary between merger and elastic scattering.

Note, in particular, that all trajectories escape to infinity or end in a merging—there exist no bound states.

We end with a brief discussion on the sequence of events that occur when two domains merge. We find numerically that when two clusters merge in a head-on collision they do so in the following stereotypic manner [Fig. 3(a) and Supplemental Material, movie 6 [27]]—(i) initial overlap of the concentration fields leads to the formation of a neck region, which develops an aster defect (ii) the neck widens to produce an elliptic domain which then (iii) relaxes

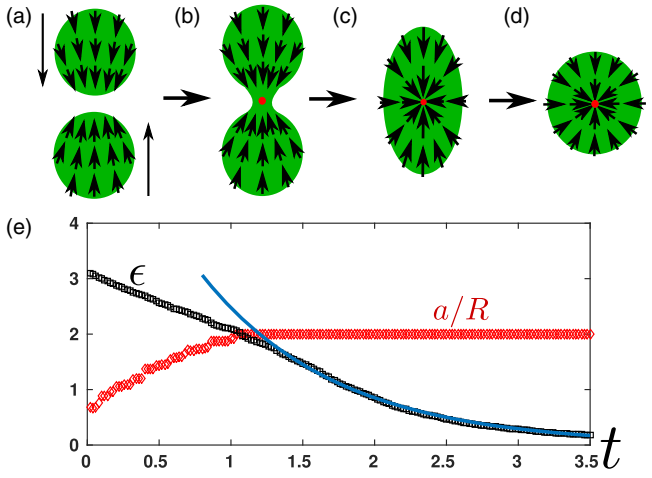

FIG. 3. A schematic of the sequence of events in merger, namely, (a) approach of the clusters, followed by (b) neck formation, which (c) grows to form an elliptic domain that (d) relaxes exponentially to a radially symmetric domain. (e) Time evolution of the ratio of the neck width a to the single domain radius R (red diamonds) as well as the shape factor $\epsilon = d_{\mathrm{maj}}/d_{\mathrm{min}} - 1$ (black squares), where d_{maj}, d_{min} are the lengths of the major and minor axes of the ellipse enclosing the merging domain area. The blue line is an exponential fit.

exponentially to a radially symmetric domain with an aster defect (as in Ref. [43]), Fig. 3(b).

When K is large the aster core is unstable [35] and moves out of the merged domain. However, when K is small, the defect core is stable and remains to form a stationary aster or spiral aster (Supplemental Material, contrast movies 4 and 5 [27]). In the intermediate regime, we find that the fate of the domain depends on the impact parameter b and the self-advection speed v_0, revealing the dynamical nature of the interacting myosin field. We will carry out a detailed study of the dynamics of merger in a later work.

In summary, we have conducted a detailed study of the form and dynamics of the compact, emergent structures that arise in a hydrodynamic description of an active polar fluid with associated "motor" elements. By explicit construction of effective equations of motion, we have demonstrated that these structures behave as extended self-propelled particles that exhibit both phoresis and taxis. We expect our results to be relevant to systems exhibiting both self-propulsion as well as contractile stresses, such as might be expected for the dynamics of actomyosin structures as the cell surface [20]. We look forward to experimental tests of our predictions in *in vivo* as well as *in vitro* contexts [44].

We thank S. Ramaswamy, K. VijayKumar, Amit Singh, B. R. Ujwal. and the members of the Simons Centre for the Study of Living Machines for insightful discussions.

*madan@ncbs.res.in

[1] P. M. Chaikin and T. C. Lubensky, *Principles of Condensed Matter Physics* (Cambridge University Press, Cambridge, England, 2000).
[2] M. F. Hagan and A. Baskaran, Curr. Opin. Cell Biol. **38**, 74 (2016).
[3] K. Kruse, J. F. Joanny, F. Julicher, J. Prost, and K. Sekimoto, Phys. Rev. Lett. **92**, 078101 (2004).
[4] M. C. Marchetti, J. F. Joanny, S. Ramaswamy, T. B. Liverpool, J. Prost, M. Rao, and R. A. Simha, Rev. Mod. Phys. **85**, 1143 (2013).
[5] T. Sanchez, D. T. N. Chen, S. J. DeCamp, M. Heymann, and Z. Dogic, Nature (London) **491**, 431 (2012).
[6] F. C. Keber, E. Loiseau, T. Sanchez, S. J. DeCamp, L. Giomi, M. J. Bowick, M. C. Marchetti, Z. Dogic, and A. R. Bausch, Science **345**, 1135 (2014).
[7] S. J. DeCamp, G. S. Redner, A Baskaran, MF Hagan, and Z. Dogic, Nat. Mater. **14**, 1110 (2015).
[8] E. Putzig, G. S. Redner, A Baskaran, and A Baskaran, Soft Matter **12**, 3854 (2016).
[9] L. M. Pismen, Phys. Rev. E **88**, 050502 (2013).
[10] L. Giomi, L. Mahadevan, B. Chakraborty, and M. F. Hagan, Phys. Rev. Lett. **106**, 218101 (2011).
[11] L. Giomi, M. J. Bowick, X. Ma, and M. C. Marchetti, Phys. Rev. Lett. **110**, 228101 (2013).
[12] L. Giomi, M. J. Bowick, P. Mishra, R. Sknepnek, and M. C. Marchetti, Phil. Trans. R. Soc. A **372**, 20130365 (2014).
[13] A. Doostmohammadi, M. F. Adamer, S. P. Thampi, and J. M. Yeomans, Nat. Commun. **7**, 10557 (2016).
[14] J. Palacci, S. Sacanna, A. P. Steinberg, D. J. Pine, and P. M. Chaikin, Science **339**, 936 (2013).
[15] I. Theurkoff, C. Cottin-Bizonne, J. Palacci, C. Ybert, and L. Bocquet, Phys. Rev. Lett. **108**, 268303 (2012).
[16] I. Buttioni, J. Bialké, F. Kümmel, H. Löwen, C. Bechinger, and T. Speck, Phys. Rev. Lett. **110**, 238301 (2013).
[17] O. Powl and H. Stark, Phys. Rev. Lett. **112**, 238303 (2014).
[18] A. M. Menzel, T. Ohta, and H. Lowen, Phys. Rev. E **89**, 022301 (2014).
[19] M. Fritzsche, A. Lewalle, T. Duke, K. Kruse, and G. Charras, Mol. Biol. Cell **24**, 757 (2013).
[20] K. Gowrishankar, S. Ghosh, S. Saha, Rumamol C., S. Mayor, and M. Rao, Cell **149**, 1353 (2012).
[21] A. Ahmadi, M. C. Marchetti, and T. B. Liverpool, Phys. Rev. E **74**, 061913 (2006).
[22] H. Y. Lee and M. Kardar, Phys. Rev. E **64**, 056113 (2001).
[23] S. Sankararaman, G. I. Menon, and P. B. S. Kumar, Phys. Rev. E **70**, 031905 (2004).
[24] D. Goswami, K. Gowrishankar, S. Bilgrami, S. Ghosh, R. Raghupathy, R. Chadda, R. Vishwakarma, M. Rao, and S. Mayor, Cell **135**, 1085 (2008).
[25] R. Raghupathy *et al.*, Cell **161**, 581 (2015).
[26] A. Das, A. Polley, and M. Rao, Phys. Rev. Lett. **116**, 068306 (2016).
[27] See Supplemental Material at http://link.aps.org/supplemental/10.1103/PhysRevLett.118.078104 for numerical details, details of the analytical calculations and movies, which includes Refs. [28,29].
[28] S. Muhuri, M. Rao, and S. Ramaswamy, Europhys. Lett. **78**, 48002 (2007).
[29] X. Yang, D. Marenduzzo, and M. C. Marchetti, Phys. Rev. E **89**, 012711 (2014).
[30] J. Toner and Y. Tu, Phys. Rev. Lett. **75**, 4326 (1995).
[31] P-G. de Gennes and J. Prost, *The Physics of Liquid Crystals* (Clarendon Press, Oxford, 1993).
[32] A. Gopinath, M. F. Hagan, M. C. Marchetti, and A. Baskaran, Phys. Rev. E **85**, 061903 (2012).
[33] B. Liebchen, D. Marenduzzo, I. Pagonabarraga, and M. E. Cates, Phys. Rev. Lett. **115**, 258301 (2015).
[34] K. Gowrishankar and M. Rao, Soft Matter **12**, 2040 (2016).
[35] D. Pettey and T. C. Lubensky, Phys. Rev. E **59**, 1834 (1999).
[36] S. A. Langer and J. P. Sethna, Phys. Rev. A **34**, 5035 (1986).
[37] R. C. Sarasij and M. Rao, Phys. Rev. Lett. **88**, 088101 (2002); R. C. Sarasij, P. Srivastava, and M. Rao, Phys. Rev. E **85**, 041920 (2012).
[38] P. Srivastava, R. Shlomovitz, N. S. Gov, and M. Rao, Phys. Rev. Lett. **110**, 168104 (2013).
[39] S. Yabunaka and N. Yoshinaga, J. Fluid Mech. **806**, 205 (2016).
[40] S. Saha, R. Golestanian, and S. Ramaswamy, Phys. Rev. E **89**, 062316 (2014).
[41] http://math.rice.edu/~dfield/dfpp.html.
[42] S. Strogatz, *Nonlinear Dynamics and Chaos* (Levant Books, Calcutta, 2007).
[43] C. P. Brangwynne, T. J. Mitchison, and A. A. Hyman, Proc. Natl. Acad. Sci. U.S.A. **108**, 4334 (2011).
[44] D. V. Koester, K. Husain, E. Iljazi, A. Bhat, P. Bieling, R. D. Mullins, M. Rao, and S. Mayor, Proc. Natl. Acad. Sci. U.S.A. **113**, E1645 (2016).